PCCP

Physical Chemistry Chemical Physics

An international journal

www.rsc.org/pccp

Volume 9 | Number 39 | 21 October 2007 | Pages 5281–5388

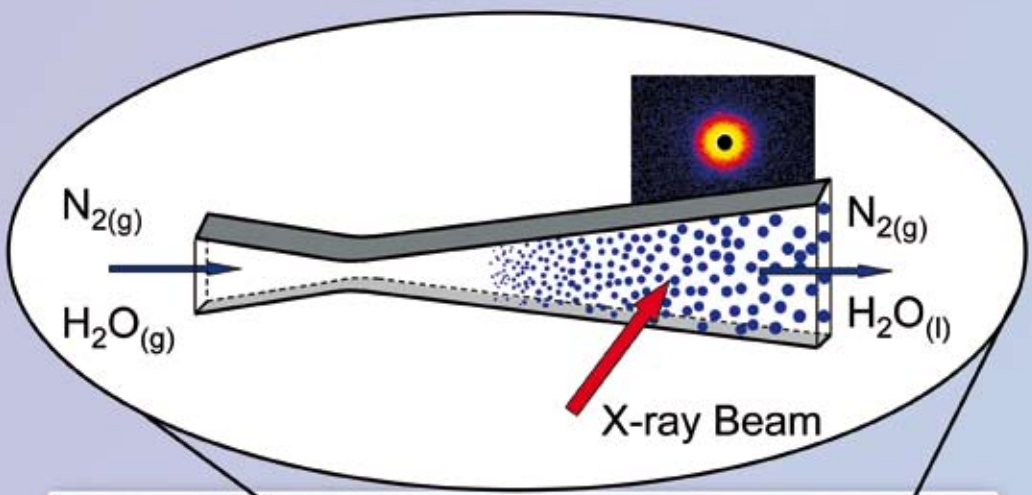

Courtesy of Argonne National Laboratory

ISSN 1463-9076

Small angle X-ray scattering measurements probe water nanodroplet evolution under highly non-equilibrium conditions†

Barbara E. Wyslouzil,*[a] Gerald Wilemski,[b] Reinhard Strey,[c] Soenke Seifert[d] and Randall E. Winans[d]

Received 20th June 2007, Accepted 20th July 2007
First published as an Advance Article on the web 14th August 2007
DOI: 10.1039/b709363b

Our *in situ* small angle X-ray scattering (SAXS) measurements yield an unprecedented and detailed view of rapidly evolving H_2O nanodroplets formed in supersonic nozzles. The SAXS experiments produce spectra in a few seconds that are comparable to small angle neutron scattering (SANS) spectra requiring several hours of integration time and the use of deuterated compounds. These measurements now make it possible to quantitatively determine the maximum nucleation and growth rates of small droplets formed under conditions that are far from equilibrium. Particle growth is directly followed from about 10 μs to 100 μs after particle formation with growth rates of $\sim$0.2 to 0.02 nm μs^{-1}. The peak H_2O nucleation rates lie between 10^{17} and 10^{18} cm^{-3} s^{-1}.

Introduction

Supersonic nozzles are a convenient way to produce and study high number density aerosols comprised of droplets in the nanometer size range.[1] With nozzle cooling rates on the order of 0.5 K μs^{-1}, the vapor reaches high supersaturations, and particle formation and growth occur far from equilibrium. Prior explorations of nanodroplet evolution in nozzles have been limited by the standard experimental techniques, including pressure measurements and light scattering,[2,3] because these techniques do not provide detailed information regarding particle size distributions. Thus, data to spur the development of better theories for nucleation, particle growth, and coagulation under highly non-equilibrium conditions are generally not available. In this paper we describe the use of small angle X-ray scattering (SAXS) to directly determine the nucleation and growth rates of nanoparticles in supersonic nozzles similar to those used previously.[4] Although these experiments focus on water nanodroplets, many of the issues we address are germane to the production of monodisperse nanoparticles by other aerosol routes.

In our earlier work[4] we used small angle neutron scattering (SANS) to characterize the D_2O aerosols formed in supersonic nozzles. In contrast to long visible light ($\sim$500 nm), the wavelengths of neutrons (0.2–1 nm) and X-rays ($\sim$0.1 nm) are smaller than the droplets (average radius $\langle r \rangle$ $\sim$10 nm). Thus, SANS and SAXS spectra have structure that can be fit to determine the mean particle radius, $\langle r \rangle$, the width of the distribution σ or its polydispersity $\xi = \sigma/\langle r \rangle$, and the number density N of the aerosol. As we show here, the small (0.2 mm × 0.2 mm), highly monochromatic ($\Delta\lambda/\lambda = 10^{-4}$) X-ray beam with its high photon flux overcomes the time and resolution limitations inherent in our SANS studies and makes detailed studies of particle formation and evolution in supersonic flows entirely practical. Our work complements that of others who have used SAXS to examine the evolution of soot[5,6] and metal oxide[7,8] nanoparticles produced in flames.

Experimental

The apparatus used in this work has been described in detail in Tanimura *et al.*[9] and is only summarized briefly here. A dilute mixture of water vapor (<6 mol%) in N_2 carrier gas, initially at stagnation pressure p_0 and stagnation temperature T_0, expands as it flows through a supersonic Laval nozzle. As the gas cools, the supersaturation increases rapidly and particles begin to form by homogeneous nucleation. Eventually, the particle formation rate is high enough that growth of the newly formed droplets rapidly depletes the vapor, and the latent heat released increases the temperature and pressure of the gas. Both effects quench nucleation, although depletion is far more important.

We characterize the condensation process by making extensive static pressure measurements along the axis of the nozzle for different combinations of T_0 and the mass flow rate of water entering the nozzle. We hold p_0 constant by reducing the flow rate of N_2 as the flow rate of water increases. For these dilute gas mixtures the total molar flow rate through the nozzle is approximately constant.[10] A dry pressure trace (N_2 flow only) defines the effective area ratio A/A^* of the nozzle. To determine the temperature, density, and velocity in the condensing flow, we integrate the diabatic flow equations[4] using the stagnation conditions, the condensing flow pressure trace, and the effective area ratio as input. We also assume that A/A^* is not affected by the condensation process. The validity

[a] *Chemical and Biomolecular Engineering Department, The Ohio State University, Columbus, OH 43210, USA*
[b] *Department of Physics, University of Missouri – Rolla, Rolla, MO 65409, USA*
[c] *Institut für Physikalische Chemie, Universität zu Köln, Köln, Germany*
[d] *X-ray Science Division, Advanced Photon Source, Argonne National Laboratory, Argonne, IL 60439, USA*

† The HTML version of this article has been enhanced with colour images.

of this assumption is discussed by Tanimura *et al.*[9] Analysis of the pressure data yields[4] the pressure and temperature corresponding to the peak nucleation rate and shows that, depending on the nozzle and flow conditions, the nucleation bursts last between 7 and 15 μs.

We investigated two Laval nozzles, H2 and C2, characterized by the effective expansion rates of $d(A/A^*)/dx = 0.054\ cm^{-1}$ and $d(A/A^*)/dx = 0.078\ cm^{-1}$, respectively. These nozzles have rectangular cross sections with a constant width equal to 1.2 cm, and the height at the throat is 0.5 cm. The top and bottom walls of the nozzle converge and diverge symmetrically. The straight converging section (~2 cm long, ~20° half angle) and the straight diverging section (~9.5 cm long, 0.89° or 1.5° half angle) are joined near the throat by a ~2.5 cm long cubic section. The cubic is chosen so that the expansion in the supersonic region is continuous through the second derivative. A photograph of a similar nozzle is given in Fig. 2 of Wyslouzil *et al.*[10] For H_2O condensation, p_0 was fixed at 30 kPa and T_0 was 298 K (nozzle H2) or 308 K (nozzle C2). A limited number of experiments were conducted with D_2O using nozzle C2 and here (p_0, T_0) = (60 kPa, 308 K). The expansion rate of nozzle C2 is very close to that of nozzle C used by Kim *et al.*,[4] and the stagnation conditions are the same. We can, therefore, directly compare the current SAXS measurements to our earlier SANS results.

All SAXS measurements were made at the Advanced Photon Source at Argonne National Laboratory on the Besserc 12-ID beam line[11] using 12 keV X-rays ($\Delta\lambda/\lambda = 10^{-4}$) and a sample to detector distance (SDD) of 2.0 m. The X-ray windows were made by machining 1 mm × 90 mm slits into the nozzle side walls and then covering these slits by gluing 25 μm thick ruby mica sheets (10 mm × 100 mm) to the inside of the aluminium side walls with epoxy.[12] The range of the momentum transfer vector q, where $q = (4\pi/\lambda)(\sin\theta/2)$ and θ is the scattering angle, was calibrated by scattering from a sample of silver behenate. We used the APS data reduction program to correct for the dark background, the pixel efficiency and spatial inhomogeneities on the detector. To produce the radially averaged spectra, the pixels were binned logarithmically (four pixels per bin) to improve the statistics, especially at high q.

Results and discussion

In Fig. 1, we directly compare our current measurements with two D_2O scattering spectra measured by Kim *et al.*[4] using SANS, after the latter have been corrected for the increased scattering length densities of X-rays over neutrons, ($\Delta\rho_{D_2O,X\text{-}ray}/\Delta\rho_{D_2O,neutron}$).[2] Because the absolute calibration procedures for SANS are more firmly established than those for SAXS, we can force agreement between the two measurements to place the SAXS results on an absolute intensity scale. The dashed lines are the X-ray data plotted on the scale used during the preliminary data evaluation. Multiplying the original SAXS data by 4.6 gives an excellent match between the SAXS and SANS data sets except in the low q region where the SANS data consistently lie above the SAXS data.[13] The difference at low q is a consequence of the effective higher polydispersity of the aerosol resulting from the 12 mm wide viewing volume in the SANS experiment *versus* the nearly point measurements in SAXS. We estimate the accuracy of our calibration procedure to be ±20% based on a ~10% uncertainty for the original NIST calibration and ~10% uncertainty in reproducing the experiments and determining the correction factor.

Each of the D_2O spectra measured using SANS required ~2 h of integration time (1 h for the sample, 1 h for the empty nozzle) at each sample to detector position. Thus, the SANS spectrum in Fig. 1(a) required 4 h of integration rather than the ~10 s (5 s sample, 5 s empty nozzle) required for the SAXS

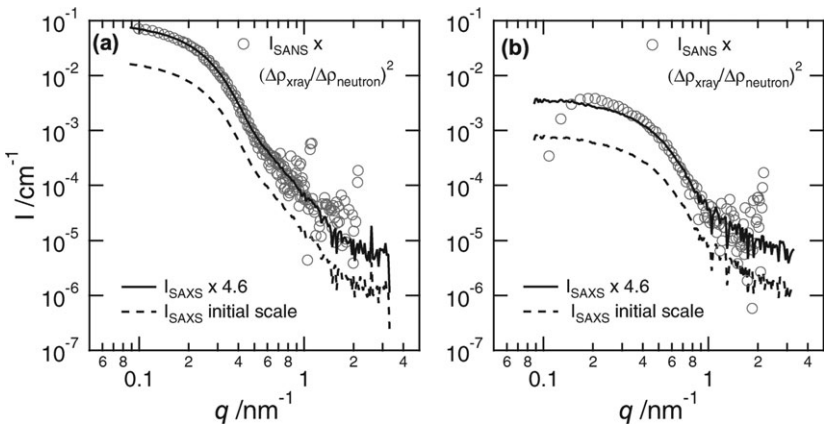

Fig. 1 The SANS and SAXS spectra for D_2O aerosols measured under nominally identical conditions agree quantitatively when the SANS data are corrected for the difference in scattering length densities of X-rays over neutrons and the SAXS data, using the initial calibration factor, are adjusted by a single multiplicative factor of 4.6. (a) $\dot{m}_{D_2O} = 8.9\ g\ min^{-1}$, (b) $\dot{m}_{D_2O} = 2.4\ g\ min^{-1}$. Error bars are omitted from the SANS data for clarity. Error bars are not shown for the X-ray spectra because even at $q > 1\ nm^{-1}$, the high X-ray flux ensures that the error bars based on count statistics are generally less than 5% of the signal. Below $q = 1\ nm^{-1}$, they are less than 1%. The apparent structure in the SAXS signal at high q is due to systematic subtraction error, for example, the sample (N_2 + D_2O droplets + D_2O vapor + windows + air scattering) are measured a few minutes before or after the empty cell (N_2 + windows + air scattering). To avoid plotting negative intensities on a log scale, we added flat backgrounds of $10^{-6}\ cm^{-1}$ ($4.6 \times 10^{-6}\ cm^{-1}$) to the SAXS spectra on the initial (corrected) scale and a flat background of $5 \times 10^{-6}\ cm^{-1}$ to the SANS spectrum.

spectrum measured at a single sample to detector position. At high water flow rates the SAXS data cover ~5 orders of magnitude in intensity over the accessible range of q. The inflection in the spectra at intermediate q corresponds to the Bessel function minimum, and in the high q region the intensity decreases as q^{-4}—features characteristic of scattering from a polydisperse distribution of spheres in bulk contrast. As the flow rate of D_2O decreases, Fig. 1b, the inflection moves to larger q and the intensity at low q drops, consistent with the expected decrease in average particle size as the volume of condensible material entering the nozzle is reduced. For nanodroplets consisting of *one component*, SAXS is clearly preferable to SANS because it is significantly faster, does not require expensive deuterated materials, and covers a wider q-range for a single detector position. Furthermore, because the speed of light is so much higher than the droplet speed, the Doppler shift correction[14] made for neutron scattering is not needed here.

Estimates for the parameters of the aerosol size distribution are easily obtained by fitting the spectra to polydisperse distributions of spheres. Here we used a Schultz distribution[15] to determine the average particle radius $\langle r \rangle$, the width of the size distribution σ and the scattered intensity as $q \rightarrow 0$, I_0. When the data are on an absolute intensity scale, the aerosol number density N is derived from I_0 using[16]

$$N = \left(\frac{3}{4\pi}\right)\left(\frac{(z+1)^5}{(z+6)(z+5)(z+4)(z+3)(z+2)}\right)\left(\frac{I_0}{\langle r\rangle^6(\Delta\rho)^2}\right)$$

where $z = (\langle r \rangle/\sigma)^2 - 1$. The error bars associated with the parameters were determined as follows. For each experimental condition we combined two 5 s sample and two 5 s local background measurements in different ways to yield 4 spectra. We then fit these spectra to determine values for $\langle r \rangle$, σ and N. We averaged the values for the fit parameters, and the error bars represent one standard deviation from the mean.

In Fig. 2 we compare the values of N, $\langle r \rangle$ and σ as a function of the D_2O mass flow rate derived from the SANS and SAXS experiments. The agreement between the two data sets, taken ~3 years apart, at different facilities and using two different detection methods is remarkable. The average particle sizes are almost identical, the values of N are close, and the widths of the distributions measured using SANS are only 12–16% higher than those measured by SAXS. One reason for the latter is the wider viewing volume used in the SANS experiments, and another, as we will show below, is the continued slow growth of the droplets, even near the nozzle exit. Thus, even with identical values of $\langle r \rangle$, contributions to the SANS scattering pattern from smaller droplets entering and larger droplets leaving the 12 mm wide viewing volume will effectively broaden the size distribution.[17]

A series of similar SAXS measurements was made for H_2O using two nozzles characterized by different expansion rates. Fig. 3 summarizes the variation in $\langle r \rangle$, σ and N at a fixed location in the nozzle with the mass flow rate of water. For both nozzles there is a systematic increase in $\langle r \rangle$ and σ and, initially, a decrease in N with $\dot{m}_{H_2O}$. Furthermore, the droplets formed in the more rapidly expanding nozzle C2 are significantly smaller, the distribution width is narrower, and the number density is higher than the droplets formed in nozzle H2. These observations are consistent with the fact that faster expansion rates lead to both higher nucleation rates and somewhat shorter nucleation bursts.[4] With a fixed initial amount of condensible material, the droplets are necessarily smaller as the number of droplets increases. In nozzle C2, the increase in N with mass flow rate at higher $\dot{m}_{H_2O}$ is unexpected, and we are exploring this effect in more detail by modelling the nucleation and growth process in our nozzles.

As illustrated in Fig. 4(a), we also characterized H_2O droplets as a function of the distance downstream of the throat at a fixed water flow rate of 5 g min^{-1}. Because the size of the X-ray beam is only 0.04 mm^2, these are essentially point measurements, and as a consequence we can easily resolve particle growth spatially, or equivalently, temporally. Note that in our nozzles, the velocity of the gas is ~400 m s^{-1}, and 1 mm corresponds to a flow time of ~2.5 μs. The pressure trace measurements corresponding to this liquid flow rate show that the peak nucleation rate occurs about ~1.5 cm downstream of the throat. Our first observation position for particles is ~2 cm downstream of the throat and, thus, we first

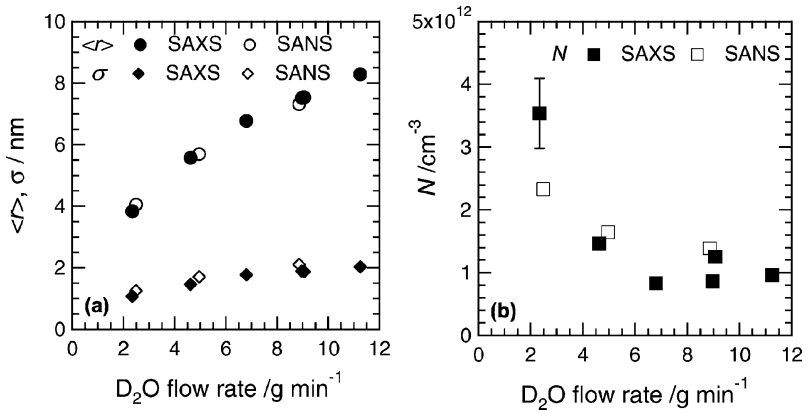

Fig. 2 The Schultz size distribution parameters, (a) average radius $\langle r \rangle$, distribution width σ, and (b) number density N, for D_2O aerosols measured ~5.6 cm downstream of the throat in nearly identical nozzles using SAXS (open symbols) and SANS (filled symbols). The error bars are only shown for points where they are larger than the symbol size. The SANS measurements[4] were made using the NG7-SANS at the NIST Center for Neutron Research.

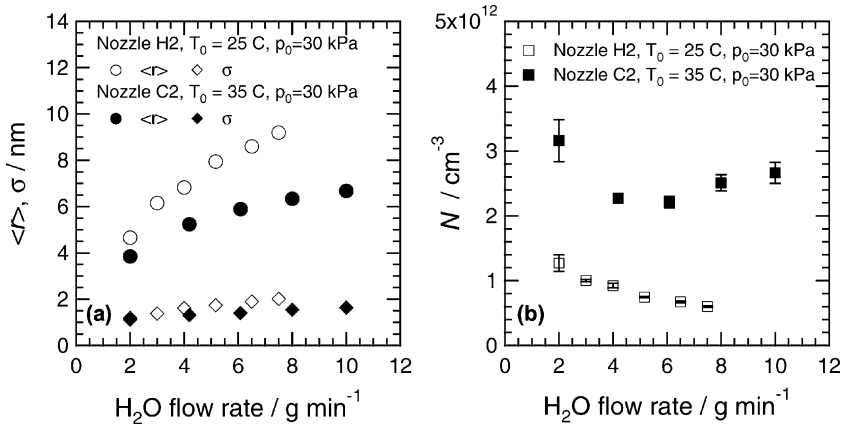

Fig. 3 (a) The average particle size and the width of the size distribution both increase with the initial mass flow rate of condensible while (b) the number density of droplets initially decreases. The measurement location is ~5.6 cm downstream of the throat. The behavior of N at higher flow rate may depend on nozzle shape and operating conditions. Nozzle C2 has a higher expansion rate, leading to higher nucleation rates, higher aerosol number densities and smaller droplet sizes than in nozzle H2.

observe droplets ~10 μs after they have formed. The mean radius $\langle r \rangle$ of the aerosol then increases from ~3.5 to 8 nm over a distance of about 3.5 cm, or in ~90 μs.

From the pressure trace measurements we also determine the local gas velocity, which allows us to convert position in the nozzle into flow time downstream of the throat. Calculating the mean droplet growth rate is then straightforward and Fig. 4(b) summarizes our results. The highest average growth rate, $(d\langle r \rangle/dt)$, of the droplets we observe here is 0.17 nm μs^{-1}. The growth rate drops to ~0.02 nm μs^{-1} within ~40 μs primarily due to vapor depletion.

In contrast to the ~200% increase in $\langle r \rangle$, the width of the distribution σ only increases about 30%, from ~1.3 to 1.7 nm, between the first and last observation points. The particle size distribution is, therefore, found to dramatically "narrow" as the aerosol evolves, *i.e.*, ξ decreases from 0.37 to 0.21. The width of the aerosol size distribution is a direct consequence of the length of the nucleation burst and the particle growth rate, since particles formed at the beginning of the nucleation burst grow significantly larger than the last particles formed. However the relative "birth advantage" is lost as the growth time increases and the average particle size gets large compared to the distribution width. For aerosols with a narrow size distribution, both coagulation and Ostwald ripening act to increase σ. Given enough time, coagulation leads to self-preserving size distributions with effective widths larger than those observed here.[19] Simple coagulation estimates[2] suggest that N should only decrease by ~5–10% as the aerosol moves through the nozzle. For monodisperse droplets coagulating in the free molecular regime, Vermury *et al.*[19] estimated the time required to reach the self preserving size distribution was 14 times that required to halve the initial number density. Thus, we expect the particles to remain relatively monodisperse as they exit the nozzle.

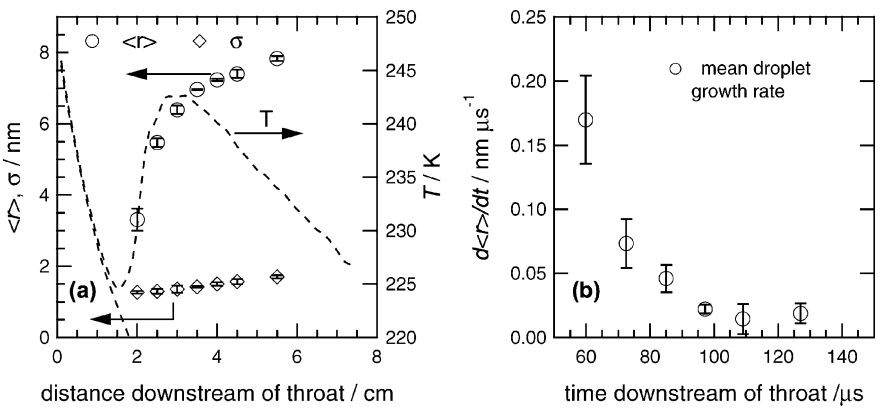

Fig. 4 In this experiment the water flow rate was 5 g min^{-1}, and T_0 and p_0 were 298 K and 30 kPa, respectively. (a) The average size $\langle r \rangle$ of H_2O droplets increases rapidly as a function of the distance downstream of the throat while the width σ of the distribution remains relatively constant. The short dashed lines are the temperatures corresponding to an isentropic expansion of the gas mixture (lower curve) and the temperature of the condensing flow (upper curve). These temperatures are derived from static pressure measurements as described in the text. The period of rapid particle growth corresponds closely to the rapid increase in temperature of the gas stream. (b) The mean droplet growth rates were calculated from adjacent observation points as the difference in the mean droplet size divided by the difference in time. The latter uses the local gas velocity that is derived from the static pressure measurements. The growth rates are plotted at the time that corresponds to the location midway between adjacent measurements.

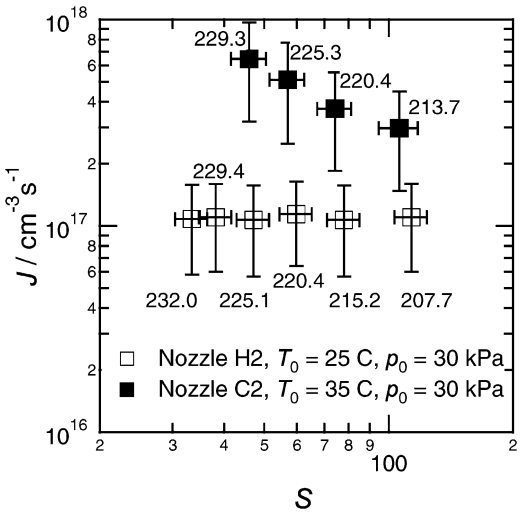

Fig. 5 The measured nucleation rates for H_2O in a supersonic nozzle as a function of supersaturation S at the indicated temperatures (K). Horizontal error bars correspond to ±1 K due to uncertainty in the temperature.

Finally, we can combine the number densities, measured by SAXS, with the characteristic time corresponding to the peak nucleation rate $\Delta t_{J_{max}}$, from axial pressure measurements, to calculate the nucleation rate using

$$J_{max}(S_{J_{max}},\ T_{J_{max}}) = \frac{N}{\Delta t_{J_{max}}} f_{exp} \qquad (1)$$

Here $S_{J_{max}}$ and $T_{J_{max}}$ are, respectively, the supersaturation and temperature corresponding to the peak nucleation rate, and $f_{exp} = \rho_{NZ}/\rho_{VV}$ accounts for the change in gas density ρ between the nucleation zone NZ and the viewing volume VV. All of these values were determined by pressure measurements as described in Kim *et al.*[4] Fig. 5 summarizes the nucleation rates determined for the H_2O experiments. In nozzle H2 the peak nucleation rate is essentially constant, consistent with the result first observed by Khan *et al.*[20] for D_2O condensation in a slightly slower nozzle. For nozzle C2, the rates are higher than in nozzle H2 and decrease by about a factor of 2 as the temperature decreases, consistent with the observations of Kim *et al.*[4] for D_2O nucleation rates in a comparable nozzle.

Summary and conclusions

We have shown that SAXS is a fine way to determine the size distributions of rapidly evolving aerosols formed in supersonic nozzles. For pure or well-mixed nanodroplets, SAXS experiments yield spectra in a few seconds that are comparable to SANS spectra requiring several hours of integration time and the use of deuterated compounds. The narrow X-ray beam also permits the size distributions of H_2O droplets to be spatially resolved along the nozzle axis, and the mean radius can be reliably determined even when the droplets are growing rapidly. These growth measurements will allow us to stringently test non-isothermal droplet growth laws under highly non-equilibrium conditions. We can also determine nucleation rates for a wide range of hydrogen-rich compounds, such as the *n*-alcohols and *n*-alkanes typically used in vapor–liquid nucleation research. The high rates characteristic of nozzles, $J \sim 10^{17}$ cm^{-3} s^{-1}, provide a stringent test of extant nucleation rate theories. Accurate nucleation and growth rate theories are needed to assist the development of challenging technical applications such as the production of metal nanoparticles in supersonic nozzles where hostile operating conditions make measurements extremely difficult.

Acknowledgements

This work was supported by the National Science Foundation under Grant numbers CHE-0410045 and CHE-0518042 and by the Donors of the Petroleum Research Fund administered by the American Chemical Society. Use of the Advanced Photon Source was supported by the US Department of Energy, Office of Science, Office of Basic Energy Sciences, under Contract No. DE-AC02-06CH11357. We acknowledge the support of the National Institute of Standards and Technology, US Department of Commerce, in providing the neutron research facilities used in this work. We thank H. Laksmono and R. Xiao for help with the pressure trace measurements.

References

1 B. E. Wyslouzil, G. Wilemski, R. Strey, C. H. Heath and U. Dieregsweiler, *Phys. Chem. Chem. Phys.*, 2006, **8**, 54.
2 C. A. Moses and G. D. Stein, *J. Fluids Eng.*, 1978, **100**, 311.
3 J. A. Clumpner, *J. Chem. Phys.*, 1971, **55**, 5042.
4 Y. J. Kim, B. E. Wyslouzil, G. Wilemski, J. Wölk and R. Strey, *J. Phys. Chem. A*, 2004, **108**, 4365.
5 J. P. Hessler, S. Seifert and R. E. Winans, *Proc. Combust. Inst.*, 2002, **29**, 2743.
6 J. P. Hessler, S. Seifert, R. E. Winans and T. H. Fletcher, *Faraday Discuss.*, 2001, **119**, 395.
7 G. Beaucage, H. K. Kammler, R. Mueller, R. Strobel, N. Agashe, S. E. Pratsinis and T. Narayanan, *Nat. Mater.*, 2004, **3**, 370.
8 H. K. Kammler, G. Beaucage, D. G. Kohls, N. Agashe and J. Ilavsky, *J. Appl. Phys.*, 2005, **97**, 054309.
9 S. Tanimura, Y. Zvinevich, B. E. Wyslouzil, M. Zahniser, J. Shorter, D. Nelson and B. McManus, *J. Chem. Phys.*, 2005, **122**, 194304.
10 B. E. Wyslouzil, C. H. Heath, J. L. Cheung and G. Wilemski, *J. Chem. Phys.*, 2000, **113**, 7317.
11 M. A. Beno, G. Jennings, M. Engbretson, G. S. Knapp, C. Kurtz, B. Zabransky, J. Linton, S. Seifert, C. Wiley and P. A. Montano, *Nucl. Instrum. Methods Phys. Res., Sect. A*, 2001, **467**, 690.
12 Making the height of the mica sheet greater than the distance separating the nozzle blocks ensures that the inner surface of the nozzle is smooth in the supersonic region and, thus, avoids introducing weak shocks into the flow. The strength of the thin mica sheets limits the height of the side wall slit to 1 mm.
13 The multiplicative factor of 4.6 was necessary because the scale used in the initial SAXS data evaluation was not based on an absolute calibration standard. The scale for the SANS data is based on an absolute calibration procedure.
14 B. E. Wyslouzil, G. Wilemski, J. L. Cheung, R. Strey and J. Barker, *Phys. Rev. E: Stat. Phys., Plasmas, Fluids, Relat. Interdiscip. Top.*, 1999, **60**, 4330.
15 M. Kotlarchyk and S. H. Chen, *J. Chem. Phys.*, 1983, **79**, 2461.
16 NG3 and NG7 30-meter SANS Instruments Data Analysis Manual, National Institute of Standards and Technology, NIST NCNR, Gaithersburg, MD, 2001, www.ncnr.nist.gov/programs/sans/manuals/data_anal.html.
17 Aerosol polydispersity may also be affected by the presence of boundary layers next to the nozzle walls. Model calculations by Schnerr *et al.*[18] found that within the boundary layer nucleation

occurred further downstream as the wall was approached. The average particle size, however, rapidly approached that of the aerosol in the main stream. Based on the measurements of Tanimura *et al*.,[9] we estimate that at most 5% of the aerosol is formed more than 1 cm downstream of the particle formation event in the main stream. The observed polydispersity, therefore, is a result of the inherent polydispersity of the aerosol, modified slightly by particle formation in the boundary layer, and of the resolution functions of the instruments including the aperture size, the wavelength distribution, and the finite pixel size. The instrument factors associated with X-ray scattering are all much smaller than those of our earlier neutron scattering studies.

18 G. H. Schnerr, R. Bohning, T. Breitling and H. A. Jantzen, *AIAA J*., 1992, **30**, 1284.

19 S. Vemury, K. A. Kusters and S. E. Pratsinis, *J. Colloid Interface Sci*., 1994, **165**, 53.

20 A. Khan, C. H. Heath, U. M. Dieregsweiler, B. E. Wyslouzil and R. Strey, *J. Chem. Phys*., 2003, **119**, 3138.

